Elastic scattering and total reaction cross sections for the ^{8}B, ^{7}Be, and ^{6}Li +^{12}C systems

A. Barioni,[1] J. C. Zamora,[1] V. Guimarães,[1] B. Paes,[2] J. Lubian,[2] E. F. Aguilera,[3] J. J. Kolata,[4] A. L. Roberts,[4] F. D. Becchetti,[5] A. Villano,[5] M. Ojaruega,[5] and H. Jiang[5]

[1]*Instituto de Física, Universidade de São Paulo P.O. Box 66318, 05389-970 São Paulo, SP, Brazil*
[2]*Instituto de Física, Universidade Federal Fluminense, 24210-340 Niterói, RJ, Brazil*
[3]*Instituto Nacional de Investigaciones Nucleares, Apartado Postal 18-1027, 11801 México, D.F., México*
[4]*University of Notre Dame, Notre Dame, 46556 Indiana, USA*
[5]*University of Michigan, Ann Arbor, 48109 Michigan, USA*

Angular distributions for the elastic scattering of ^{8}B, ^{7}Be, and ^{6}Li on a ^{12}C target have been measured at $E_{\text{lab}} = 25.8$, 18.8, and 12.3 MeV, respectively. The analyses of these angular distributions have been performed in terms of the optical model using Woods-Saxon and double-folding type potentials. The effect of breakup in the elastic scattering of ^{8}B + ^{12}C is investigated by performing coupled-channels calculations with the continuum discretized coupled-channel method and cluster-model folding potentials. Total reaction cross sections were deduced from the elastic-scattering analysis and compared with published data on elastic scattering of other weakly and tightly bound projectiles on ^{12}C, as a function of energy. With the exception of ^{4}He and ^{16}O, the data can be described using a universal function for the reduced cross sections.

I. INTRODUCTION

Nuclei far from stability exhibit interesting features that are strongly influenced by the very low energy that binds the system. Elastic scattering measurements at low energies (near to or above the Coulomb barrier) have been used as an effective tool to investigate the unusual features of exotic nuclei, such as extended halos or neutron skins. Particular interest has been devoted to ^{6}He and ^{8}B nuclei mainly due to the availability of low-energy radioactive beams of these elements [1–6]. The exotic structure of these light nuclei alters the elastic scattering due to competing mechanisms such as breakup and transfer reactions. Due to the lower binding energy of the weakly bound light nuclei, breakup can become an important competing mechanism even at relatively low incident energies, and coupled-channels analysis is required. The importance of these couplings is well known in the investigation of elastic scattering of the neutron-rich nucleus ^{6}He on different targets such as ^{209}Bi [7], ^{120}Sn [6], and ^{64}Zn [8] and it is found to be less important in light targets such as ^{27}Al [3] and ^{12}C [9]. While many experimental data are available for the neutron-rich nucleus ^{6}He, elastic-scattering data for the proton-rich ^{8}B nucleus are rather scarce. Some high-energy experiments have been reported for ^{8}B on a ^{12}C target [10,11]. However, it is not clear if it is possible to obtain information on the halo properties of the projectile from high-energy data because those properties are, in principle, surface effects. More recently, elastic-scattering measurements for ^{8}B and ^{7}Be on ^{58}Ni have been reported [5]. Their analysis has shown striking evidence for a proton halo in ^{8}B, where projectile breakup was assumed to be responsible for the increase of the observed reaction cross section [12]. Here, as a complement to a systematic study for the elastic scattering of ^{8}B on different targets, we report the measurement and analysis of the elastic-scattering angular distributions of ^{8}B, as well as ^{7}Be and ^{6}Li, on a lighter target, ^{12}C. Nuclear effects

are expected to be more important for a lighter target, rather than the dominant Coulomb effects expected for heavier-mass targets.

The organization of this paper is as follows: In Sec. II, we describe the details of the experiment. The optical-model and double-folding model used to describe the elastic-scattering data are discussed in Sec. III, where continuum discretized coupled-channel (CDCC) calculations are presented. The energy dependence of the reaction cross sections for these systems is investigated and the results are discussed in Sec. IV. Finally, further discussion and conclusions are presented in Sec. V.

II. THE EXPERIMENT

The elastic-scattering angular distributions of ^{8}B, ^{7}Be, and ^{6}Li on a natural carbon target were measured at $E_{\text{lab}} = 25.8$, 18.8, and 12.3 MeV, respectively. The secondary ^{8}B and ^{7}Be radioactive ion beams, together with the contaminant ^{6}Li ions, were simultaneously produced by the *TwinSol* system installed at University of Notre Dame [13]. The in-flight beams were produced by impinging a 35-MeV primary ^{6}Li^{3+} beam on a ^{3}He gas-cell production target. The ^{3}He gas cell was kept at a pressure of 1 atm and was mounted in a small (20 cm in diameter) chamber just before the first solenoid. After crossing the production target, the ^{6}Li primary beam is stopped in a tungsten alloy and carbon Faraday cup, which allows one to integrate its charge and measure its intensity. The secondary beams produced in the forward direction are collected within an angular range of $2.7° < θ < 6°$ by the two superconducting solenoids and focused at a secondary scattering chamber. A system of blocks and collimators, located along the solenoid axes, is used to clean up the beam of interest. Although the magnetic field of the solenoids was adjusted to focus the ^{8}B secondary beam and the blocks and collimator were used to

prevent particles with different magnetic rigidity from reaching the scattering target, particles with the same magnetic rigidity such as ^{7}Be and ^{6}Li (as inelastic-scattered primary beam) also were present. The average primary beam intensity during the measurements was about 600 enA producing ^{8}B, ^{7}Be, and ^{6}Li beams of 5×10^4, 1×10^5 and 2×10^8 pps, respectively. The carbon target (99.8% ^{12}C) used in the measurements was a natural foil 1.1 mg/cm^2 in thickness mounted in a target holder. A thin gold target 2.0 mg/cm^2 in thickness also was mounted in the holder and used in separate runs to obtain the overall normalization. The lastic scattering of these beams on the gold target at these energies is expected to be Rutherford.

The scattered particles were detected by one ΔE-E Si telescope and two silicon planar E detectors covering the angles 15°, 20°, 25°, 30°, and 35° in the laboratory system. Cross sections at 45° and 50° also were obtained for the ^{6}Li beam. The telescope consisted of a 20-μm Si ΔE detector with an area of 300 mm^2 backed by a 1000-μm-thick Si E detector and had a circular aperture that subtended a solid angle of 13 msr ($\pm 3.5°$). The E detectors were 1000-μm-thick planar detectors that subtended a solid angle of 8 msr ($\pm 3.0°$). Since the elastic cross sections in the angular interval covered by these detectors could vary by up to one order of magnitude, the average detection angle was determined by a Monte Carlo simulation, which took into account the detector collimator, the secondary beam-spot dimension on the secondary target (4 mm), the secondary beam divergence (2° to 4°), and the angular distribution in the range of the detector aperture (Rutherford for the gold target and calculated in an iterative way for the ^{12}C target). This correction is particularly important for the most forward angles.

The different scattering particles were identified using the combination of ΔE and E_{total} information for the data taken with the telescope, and time-of-flight (TOF) and E_{total} for the data taken only with the E-silicon detectors. The TOF corresponded to the time interval between the radio frequency (RF) of the pulsed beam (100-ns intervals) and the fast time signal from the E detectors. A selected particle identification spectrum (TOF vs E_{total}) is shown in Fig. 1. In this plot, the scattered ^{8}B, ^{7}Be, and ^{6}Li beams on the gold target at 15° are displayed and clearly separated and identified. Some lighter particle contaminants such as ^{4}He and pileup of the intense ^{6}Li beam contaminant also can be seen in this spectrum. Owing to its limited intensity, the yield for the ^{7}Be beam was observed only for four angles.

The experimental resolution for these beams was about 800 keV, obtained from the FWHM of the peak corresponding to the scattering in the gold target. The ^{8}B and ^{6}Li nuclei have no bound excited states and the data then are purely elastic. The inelastic scattering to the first excited state ($E_x = 0.43$ MeV) of ^{7}Be is expected to be very small for the carbon target and any corresponding yield is thus included in the elastic peak.

The experimental differential cross sections of the elastic-scattering process for all three systems investigated are displayed in Figs. 2, 3, and 4, respectively. The uncertainties in the differential cross sections were estimated considering the statistical uncertainty in the yields, uncertainty in the target thickness (10%), and uncertainty in the secondary beam intensity (10%).
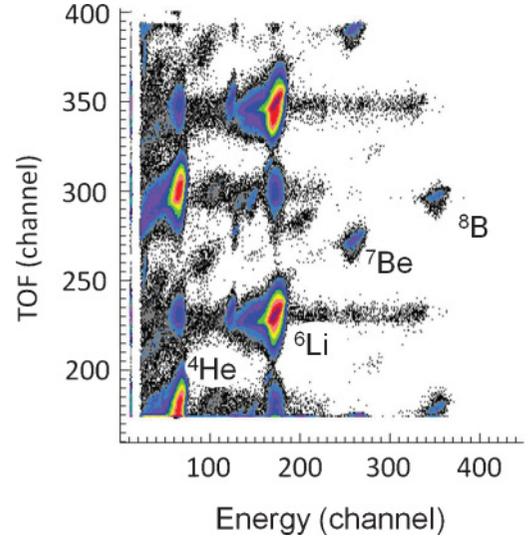

FIG. 1. (Color online) Selected particle identification spectrum (TOF vs E) for the interaction of ^{8}B, ^{7}Be, and ^{6}Li + ^{197}Au measured at 15°. The elastically scattered ^{8}B, ^{7}Be, and ^{6}Li particles are indicated, as well as ^{4}He and some other lighter particle contamination in the *TwinSol* secondary beam.

A. Optical-model calculations

Optical-model analyses of the data were carried out with the code FRESCO [14]. First, the data were analyzed in terms of conventional optical-model (OM) calculations using both volume type Woods-Saxon (WS) and double-folding nuclear potentials (plus Coulomb potentials due to uniform charged spheres). The WS potential parameters are listed in Table I and were taken from Refs. [15–17]. The results of the OM calculations can be seen in Figs. 2, 4, and 5 for each system. The curve indicated as the SPP corresponds to OM figures calculations using the SPP [18], which is a double-folding potential with energy dependence and nonlocality correction. The corresponding S-Matrix for these calculations are shown in Figs. 3, 6 and 7. For this potential, the average diffuseness for the charge and matter distributions is $a = 0.53$ fm and $a = 0.56$ fm, respectively. Within the context of the systematics
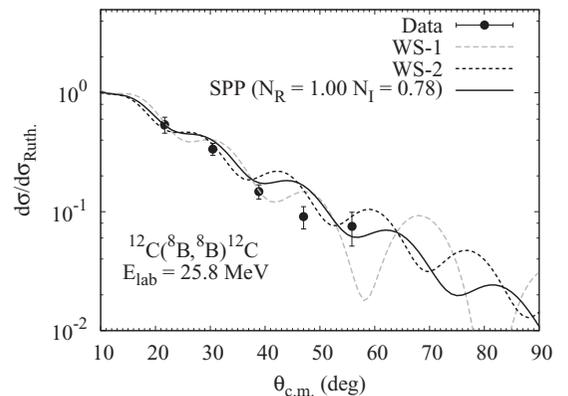

FIG. 2. The differential cross sections for the elastic scattering ^{12}C(^{8}B,^{8}B)^{12}C at 25.8-MeV incident laboratory energy. The curves are OM calculations with the parameters listed in Table I.

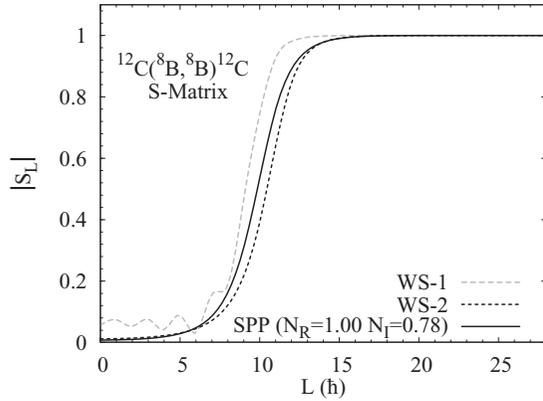FIG. 3. S matrix calculated for the elastic scattering ^{12}C(^{8}B,^{8}B)^{12}C at 25.8-MeV incident laboratory energy using the OM parameters listed in Table I.

FIG. 4. The differential cross sections for the elastic scattering ^{12}C(^{7}Be,^{7}Be)^{12}C at 18.8-MeV incident laboratory energy. The curves are OM calculations with the parameters listed in Table I.

for the densities, the SPP has no adjustable parameters. The imaginary part of the potential has the same form factor as the real part but with a normalization of $N_I = 0.78$. The SPP reproduces quite well the absolute normalization, which is of some interest considering that this folding-model potential has no free parameters as noted. Although there was no attempt to adjust the parameters to fit the data, the calculations with all of these potentials give a good description of the elastic-scattering data at forward angles.

III. CDCC CALCULATIONS

One can infer from the results in the previous section that the effect of the breakup process on the elastic scattering of ^{8}B on ^{12}C probably will be weak. This conclusion comes from the fact that there is no need for changing the normalization coefficients of the SP potential from the conventional values ($N_r = 1.0$ and $N_i = 0.78$, corresponding to the real and imaginary parts of the potential, respectively) to describe the elastic-scattering angular distributions. In this section we perform CDCC calculations for this system to study this conclusion in more detail. In the CDCC calculation, we consider a cluster model, in which the proton halo ^{8}B nucleus is represented by ^{7}Be $+ p$ in describing the interaction with the ^{12}C target. The SPP has been used to describe the real part of the interaction of the ^{7}Be core and the valence particle (the proton), where in the present calculations the core was considered inert. We used the same real part of the SPP for
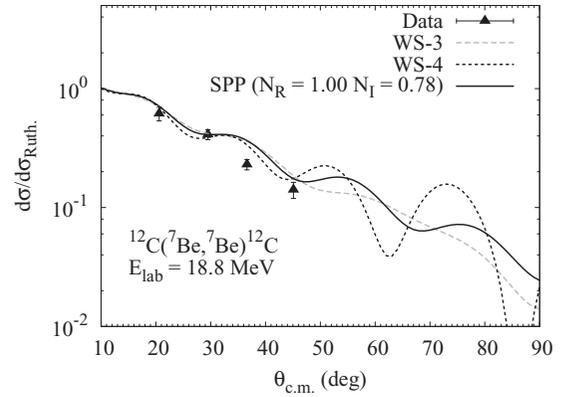
the imaginary part, again multiplied by 0.78. It has been shown that this prescription provides a good description of the elastic-scattering cross-section data for a wide energy range and for a variety of systems [19]. It is important to mention that this imaginary potential not only accounts for the absorption of flux, from the breakup to the fusion channel, but also accounts, effectively, for the inelastic excitation of the target. The p-^{7}Be interaction potential [20] used to generate the bins was the same as the one used in Refs. [12,21], where a good description of the breakup angular distribution, emission-energy distribution, and elastic-scattering distributions for the ^{8}B $+ ^{58}$Ni system was obtained.

In the CDCC calculations, the continuum states are approximated by a set of square-integrable wave functions constructed by linearly combining the p-^{7}Be elastic-scattering wave functions. To guarantee the convergence of the CDCC calculations for this system, bins up to $\epsilon_{max} = 5$ MeV and orbital angular momenta of the p-^{7}Be relative motion up to $l = 3\hbar$ were needed. To calculate the transition matrix elements between the bin states, the radial integration was extended up to $r_{bin} = 70$ fm. The projectile-target relative motion wave functions were expanded in partial waves up to $L_{max} = 200\hbar$. The interaction potential was expanded up to its quadrupole term.

In Fig. 8 we show the results of the present CDCC calculations. The solid curve represents the full CDCC calculation including all reorientation terms, both Coulomb and nuclear interactions, and all continuum-continuum couplings. The

TABLE I. Optical-model potential parameters used in the calculations. Radii are given by $R_x = r_x \times (A_P^{1/3} + A_T^{1/3})$. The depths are in MeV, and the radius and diffuseness are in fm.

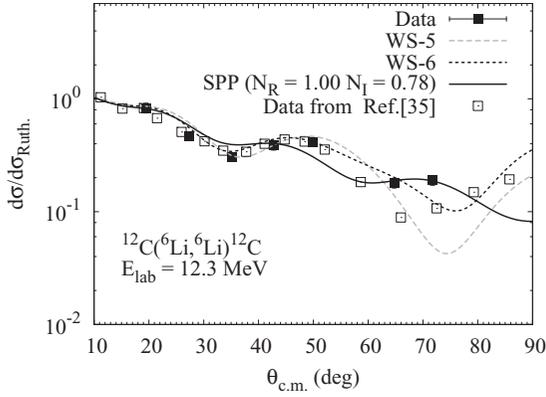| Potential	V	r_V	a_V	W_V	W_S	r_W	a_W	r_C	Reference
WS-1	245.70	0.75	0.70	11.40	–	1.17	0.49	1.24	^{6}Li + ^{12}C (24 MeV) [15]
WS-2	60.00	1.18	0.60	32.60	–	1.18	0.60	0.63	^{9}Be + ^{12}C (26 MeV) [16]
WS-3	152.00	0.65	0.77	8.55	–	1.22	0.89	0.59	^{7}Li + ^{12}C (21 MeV) [17]
WS-4	100.00	1.19	0.50	10.00	–	1.34	0.22	1.45	^{10}B + ^{12}C (18 MeV) [17]
WS-5	136.80	0.85	0.64	–	7.75	0.80	0.77	0.85	^{6}Li + ^{12}C (13 MeV) [17]
WS-6	248.50	0.78	0.70	4.72	–	1.52	0.35	1.29	^{6}Li + ^{12}C (13.0 MeV) [15]

FIG. 5. *S* matrix calculated for the elastic scattering ^{12}C(^{7}Be,^{7}Be)^{12}C at 18.8-MeV incident laboratory energy using the OM parameters listed in Table I.

continuum-continuum couplings shown are important in accurately describing the elastic-scattering angular distributions [22]. The dashed curve represents the no-coupling calculations where the OM potential is obtained by the single folding of the full Coulomb + nuclear interaction over the ^{8}B ground state, the $1p_{3/2}$ state. One can see that the agreement of the CDCC calculations with experimental data is quite good. Note that in this calculation, once we have chosen the optical potential, there again are no free parameters. Comparing the dashed and full curves one can indeed conclude that as expected the effect of the breakup channel on the elastic scattering in this energy regime in this system is indeed weak.

IV. TOTAL REACTION CROSS SECTIONS

An additional important piece of information that can be deduced from the elastic-scattering analysis is the total reaction cross section. This information is useful to investigate the role of breakup (or other reaction mechanisms) for weakly bound, exotic nuclei. If we consider different systems with different breakup threshold energies, for instance, the role of breakup can be investigated by plotting the total reaction cross
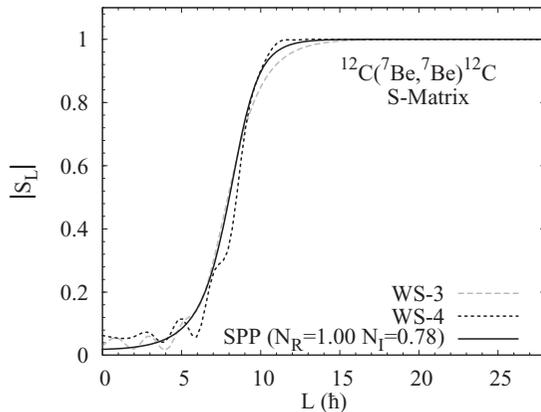

FIG. 6. The differential cross sections for elastic scattering ^{12}C(^{6}Li,^{6}Li)^{12}C at 12.3-MeV incident laboratory energy. The curves are OM calculations with the parameters listed in Table I.

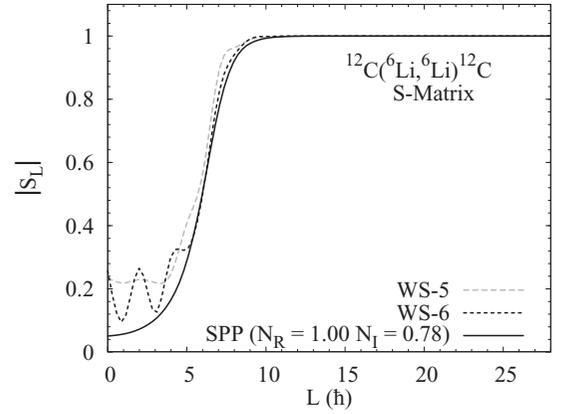FIG. 7. *S* matrix calculated for the elastic scattering ^{12}C(^{6}Li,^{6}Li)^{12}C at 12.3-MeV incident laboratory energy using the OM parameters listed in Table I.

section for weakly and tightly bound nuclei on the same target nucleus as a function of energy. To compare the cross sections for systems with different Coulomb barriers and different geometry, it is necessary to suppress the differences arising from the sizes and charges of the systems. We use a reduction procedure suggested by Gomes *et al.* [23] to do this. The reduced cross sections and energies are given by

$$\sigma_{\rm red} \rightarrow \frac{\sigma_R}{\left(A_p^{1/3} + A_t^{1/3}\right)^2} \quad {\rm and} \quad E_{\rm red} \rightarrow E_{\rm cm}\frac{\left(A_p^{1/3} + A_t^{1/3}\right)}{Z_p Z_t},$$
(1)

with $Z_P(Z_T)$ and $A_P(A_T)$ standing for the charge and mass of the projectile (target), respectively. Gomes *et al.* [23] in this way claim that the geometrical effects (such as masses and charges of the collision partners) are removed while possible anomalous values of the reduced radius r_0, which could be related to the physical processes or specific feature of the projectile nuclear matter density to be investigated, are not washed out. Figure 9 shows the results of the reduced total reaction cross sections, $\sigma_{\rm red}$, for many of the systems listed
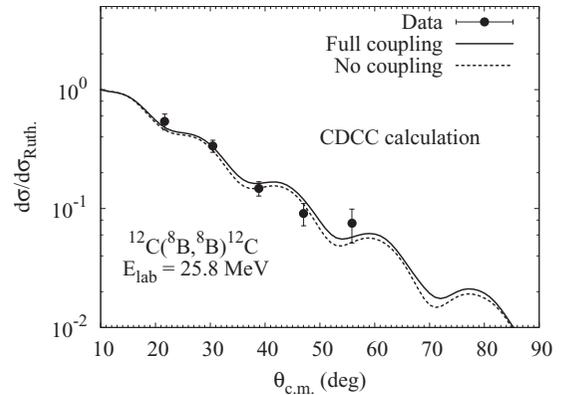

FIG. 8. The differential cross sections for the elastic scattering ^{12}C(^{8}B,^{8}B)^{12}C at 25.8-MeV incident laboratory energy. The dashed curve is the cluster-folding parametrization of the interaction without the couplings to the continuum, while the solid line is the result of the CDCC couplings.

TABLE II. Data and parameters used to determine the universal function $F(x)$, and reduced reaction cross sections as described in the text. The energies, potentials, and $\hbar\omega$ are in MeV, the radii in fm, and the cross sections in mb.

System	$E_{c.m.}$	R_B	V_B	$\hbar\omega$	σ_R	N_i	x	$F(x)$	E_{red}	σ_{Red}	Ref.
^{6}He + ^{12}C	5.86	8.04	1.98	2.64	1206.0	0.78	3.79	19.28	2.00	71.52	[24]
^{6}He + ^{12}C	6.12	8.04	1.98	2.65	1226.0	0.78	1.46	8.24	2.09	72.71	[24]
^{6}He + ^{12}C	6.60	8.04	1.98	2.65	1189.0	0.78	1.56	8.75	2.26	70.52	[25]
^{6}He + ^{12}C	12.0	8.03	1.98	2.65	1368.0	0.70	1.74	9.15	4.10	81.13	[26]
^{6}Li + ^{12}C	3.0	7.83	3.06	2.58	169.4	0.78	−0.02	0.64	0.68	10.05	[27]
^{6}Li + ^{12}C	6.0	7.83	3.06	2.59	891.3	0.80	1.14	6.74	1.37	52.86	[28]
^{6}Li + ^{12}C	16.0	7.82	3.06	2.36	1288.0	0.78	5.48	28.52	3.65	76.39	[29]
^{6}Li + ^{12}C	20.0	7.81	3.07	2.55	1292.0	0.75	6.65	33.27	4.56	76.63	[29]
^{7}Li + ^{12}C	2.84	7.95	3.01	2.76	139.4	0.78	−0.06	0.45	0.66	7.90	[29]
^{7}Li + ^{12}C	4.70	7.97	3.00	2.76	715.0	0.78	0.67	4.16	1.10	40.49	[28]
^{7}Li + ^{12}C	6.95	7.95	3.01	2.75	1071.0	0.88	1.42	8.51	1.62	60.66	[28]
^{7}Li + ^{12}C	8.21	7.95	3.01	2.75	1160.0	0.80	1.89	10.95	1.92	65.70	[28]
^{7}Li + ^{12}C	9.47	7.95	3.01	2.75	1248.0	0.94	2.34	13.58	2.21	70.68	[28]
^{7}Li + ^{12}C	13.26	7.95	3.01	2.75	1336.0	0.84	3.72	20.36	3.09	75.66	[28]
^{8}Li + ^{12}C	14.34	8.03	2.97	2.92	1405.0	0.78	3.90	21.45	3.42	76.37	[30]
^{7}Be + ^{12}C	11.87	7.77	4.11	2.69	1138.0	0.78	2.89	16.66	2.08	64.45	Present work
^{8}B + ^{12}C	15.48	7.74	5.16	2.80	1171.0	0.78	3.69	21.62	2.21	63.65	Present work
^{9}Be + ^{12}C	11.40	7.98	3.99	3.04	1289.0	0.96	2.64	15.97	2.19	67.52	[16]
^{9}Be + ^{12}C	14.90	7.98	3.99	3.03	1381.0	0.99	3.60	21.34	2.71	72.34	[16]
^{11}B + ^{12}C	5.40	8.02	4.95	3.34	298.0	1.00	0.13	1.50	0.81	14.63	[31]
^{11}B + ^{12}C	6.50	8.02	4.95	3.34	573.8	1.00	0.46	3.47	0.98	28.17	[31]
^{11}B + ^{12}C	7.20	8.02	4.95	3.34	716.4	1.00	0.67	4.80	1.08	35.17	[31]
^{11}B + ^{12}C	8.6	8.02	4.95	3.34	930.6	1.00	1.09	7.44	1.29	45.69	[31]
^{11}B + ^{12}C	11.5	8.02	4.95	3.34	1192.0	1.00	1.96	12.75	1.73	58.52	[31]
^{11}B + ^{12}C	14.00	8.02	4.95	3.34	1361.0	1.00	2.71	17.72	2.11	66.82	[31]
^{11}B + ^{12}C	26.00	8.02	4.95	3.34	1582.0	1.00	6.30	38.26	3.91	77.67	[31]

in Table II, plotted as a function of the reduced energy. The total reaction cross section for each system listed in Table II , for consistency, was obtained by performing a reanalysis of the elastic-scattering angular distributions using the double-folding SPP. However, the total reaction cross sections obtained from the present reanalysis are not very different from the ones obtained with WS potentials in the original papers. The total reaction cross section for all these systems has been obtained using the double-folding SPP with normalization of the real part fixed to $N_R = 1.00$ and the imaginary part multiplied by variable N_I values as listed in Table II.

As suggested by Kolata and Aguilera [32] and Aguilera *et al.* [33], these data can be compared with the total reaction cross section given by the Wong [34] cross section σ_R^W,

$$\sigma_R^W = R_B^2 \frac{\hbar\omega_0}{2E} \ln\left[1 + \exp\left(\frac{2\pi(E - V_B)}{\hbar\omega_0}\right)\right], \quad (2)$$

which also is reduced to

$$\sigma_{red}^W = \frac{\epsilon_0 r_0^2}{2E_{red}} \ln\left[1 + \exp\left(\frac{2\pi(E_{red} - V_{red})}{\epsilon_0}\right)\right], \quad (3)$$

where the cross sections are in fm^2 and $R_B = r_0(A_p^{1/3} + A_t^{1/3})$, $\epsilon_0 = \hbar\omega_0 \frac{(A_p^{1/3} + A_t^{1/3})}{Z_p Z_t}$, and $V_{red} = V_0 \frac{(A_p^{1/3} + A_t^{1/3})}{Z_p Z_t}$ are denoted as the Wong-model parameters. These are free parameters, and when we adjust this curve to the data for ^{6}He, ^{6}Li, ^{7}Li, ^{7}Be, ^{8}Li, ^{8}B,

^{9}Be, and ^{11}B we get $V_{red} = 0.64(3)$, $r_0 = 1.73(2)$ fm, and $\epsilon_0 = 0.43$. In particular, the value $r_0 = 1.73(2)$ fm is significantly larger than the typical values of 1.4–1.5 fm. The result of this fit is shown in Fig. 9 as the solid curve and the values obtained for the Wong-model parameters seem to be comparable with the ones obtained by Aguilera *et al.* [33] for heavier targets.
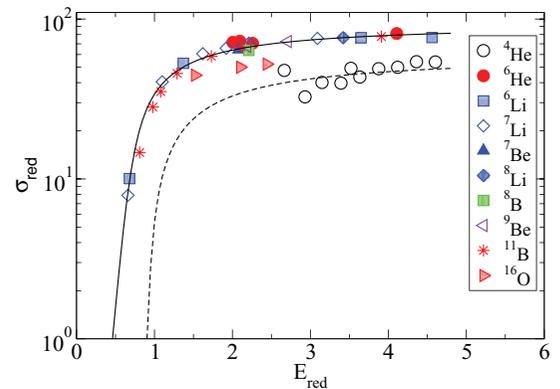

FIG. 9. (Color online) The reduced reaction cross sections for the ^{8}B + ^{12}C system obtained in this work together with reduced reaction cross sections of the lithium isotopes and some other weakly bound and tightly bound projectiles on ^{12}C. The solid and dotted line curves are explained in the text.

It has been observed for heavier targets such as ^{58}Ni, ^{64}Zn, or even ^{209}Bi, where the Coulomb breakup predominates over the nuclear breakup, that larger reduced total reaction cross sections are obtained at energies around the Coulomb barrier for exotic nuclei (^{6}He and ^{8}B) followed by the weakly bound nuclei (^{6}Li, ^{7}Li, ^{8}Li, and ^{9}Be) and then the tightly bound nuclei (^{16}O and ^{4}He) which produce the smallest total reaction cross section [32,33]. It seems that the effect of the weak binding energy is switching on additional channels that would enhance the total reaction cross sections, and the halo states do provide a related threshold effect. On other hand we can conclude that, for a target as light as ^{12}C, the additional channels would not be switching on as easily as for heavier targets, and the reduced reaction cross sections for exotic and weakly bound nuclei as well as for a tightly bound nuclei (^{11}B) follow the same trend. The exceptions are for the ^{4}He and ^{16}O projectiles. As one can see in Fig. 9, the reduced cross section for ^{4}He follows a different trend. Using the same Wong-model parameters obtained by Aguilera *et al.* in Ref. [33] for ^{4}He, i.e., $V_{\text{red}} = 0.913(5)$, $r_0 = 1.39(5)$ fm, and $\epsilon_0 = 0.175(6)$, we obtained the dashed line curve in Fig. 9. We should emphasize here that the data set for ^{4}He + ^{12}C could not be reanalyzed in terms of the double-folding SSP. Instead we use the reaction cross section from Ref. [35], where to fit the angular distributions the authors applied a smooth-cutoff model modified to include resonances of the compound nucleus ^{16}O.

Because the above renormalization (reduction) assumes that the barrier parameters depend only on the atomic and mass numbers, the behavior observed in Fig. 9 may indicate that static effects and/or dynamic effects due to breakup are also present. According to Refs. [33,36], dynamic effects would be more important in the region near to and below the reduced barrier, and static effects would be relevant for all energies. It would be interesting if one could disentangle these effects by considering another way to renormalize (reduce) the data. Canto *et al.* [37] suggested the use of a universal function $F(x)$, where static effects arising from the weakly bound nuclei would be taken into account by considering the characteristics

of the barrier for each system. The original idea was developed for fusion processes, where the fusion function is defined as

$$F(x) = \frac{2E}{\hbar\omega R^2}\sigma_F, \tag{4}$$

with

$$x = \frac{E - V_B}{\hbar\omega}, \tag{5}$$

where V_B, R_B, and $\hbar\omega$ are the height, radius, and curvature of the barrier, respectively, and σ_F is the fusion cross section.

This universal fusion function (UFF) is derived from Wong's approximation [34]:

$$\sigma_F^W = R_B^2 \frac{\hbar\omega}{2E} \ln\left[1 + \exp\left(\frac{2\pi(E - V_B)}{\hbar\omega_0}\right)\right], \tag{6}$$

which, when valid, reduces the fusion function to

$$F_0(x) = \frac{2E}{\hbar\omega_0 R_B^2}\sigma_F^W = \ln[1 + e^{(2\pi x)}] \tag{7}$$

Shorto *et al.* [38] proposed to use the parametrization of Eq. (4) to analyze reaction cross sections by replacing the fusion cross section (σ_F) by the total reaction cross section (σ_R). Thus, considering the real part of the potential, we assumed that the sum of the nuclear and the Coulomb potentials near the barrier is described by a parabola:

$$\begin{aligned} V(r) = {} & V(R_B) + \frac{1}{1!}\frac{dV(R_B)}{dr}(r - R_B) \\ & + \frac{1}{2!}\frac{d^2V(R_B)}{dr^2}(r - R_B)^2 + \ldots \simeq V_B \\ & + \frac{1}{2}\mu\omega_0^2(r - R_B)^2. \end{aligned} \tag{8}$$

To find the parameters R_B, V_B, and ω_O we then fitted the real part of the OM potential by a parabola. As indicated before, we reanalyzed all the angular distributions for the systems listed in Table II with the SPP to obtain the reaction cross section. With this potential in hand, we fit a parabola to the real part near the barrier to obtain the parameters R_B, V_B, and ω for

TABLE III. Data and parameters used to determine the universal function $F(x)$, and reduced reaction cross sections as described in the text. The energy potentials and $\hbar\omega$ are in MeV, the radii in fm, and cross sections in mb. The notation WS and WS + Res. correspond to a Woods-Saxon and Woods-Saxon plus resonance analysis, respectively.

| System	$E_{\text{c.m.}}$	R_B	V_B	$\hbar\omega$	σ_R	N_i	x	$F(x)$	E_{red}	σ_{red}	Ref.
^{4}He + ^{12}C	8.25	7.10	2.35	3.54	717.0	WS + Res.	–	–	2.67	47.70	[35]
^{4}He + ^{12}C	9.08	7.10	2.35	3.54	490.0	WS + Res.	–	–	2.93	32.60	[35]
^{4}He + ^{12}C	9.75	7.10	2.35	3.54	603.0	WS + Res.	–	–	3.15	40.12	[35]
^{4}He + ^{12}C	10.50	7.10	2.35	3.54	597.0	WS + Res.	–	–	3.39	39.72	[35]
^{4}He + ^{12}C	11.25	7.10	2.35	3.54	662.0	WS + Res.	–	–	3.63	43.88	[35]
^{4}He + ^{12}C	12.00	7.10	2.35	3.54	735.0	WS + Res.	–	–	3.88	48.90	[35]
^{4}He + ^{12}C	12.75	7.10	2.35	3.54	750.0	WS + Res.	–	–	4.12	49.90	[35]
^{4}He + ^{12}C	13.50	7.10	2.35	3.54	813.0	WS + Res.	–	–	4.36	54.09	[35]
^{4}He + ^{12}C	14.25	7.10	2.35	3.54	810.0	WS + Res.	–	–	4.60	53.89	[35]
^{16}O + ^{12}C	17.30	8.1	8.11	6.04	1029.0	WS	1.52	9.00	1.73	44.50	[39]
^{16}O + ^{12}C	20.80	8.1	8.11	6.04	1155.0	WS	2.10	12.16	2.08	49.95	[39]
^{16}O + ^{12}C	22.80	8.1	8.11	6.04	1207.0	WS	2.44	13.94	2.28	52.19	[39]
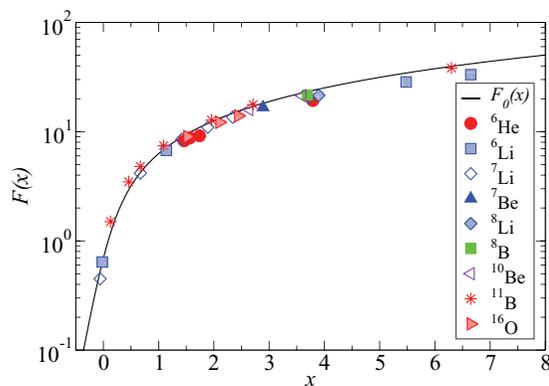
FIG. 10. (Color online) The reduced reaction cross sections considering the universal function $F(x)$ for the ^{8}B + ^{12}C system obtained in this work together with $F(x)$ of the lithium isotopes and some other weakly bound and tightly bound projectiles on ^{12}C. The solid curve is explained in the text.

each system. Using these parameters we then deduced the universal function $F(x)$ for each system. The universal functions obtained, as well as the barrier parameters for different systems from the literature and for our data, are listed in Tables II and III. The universal function $F(x)$ as a function of the parameters x can be seen in Fig. 10. Among these systems we have combinations both with weakly bound nuclei projectiles, such as ^{6,7,8}Li, ^{9}Be, and ^{6}He, and more tightly bound nuclei projectiles, such as ^{16}O and ^{11}B. The solid curve in Fig. 10 corresponds to the function $F_0(x) = \ln[1 + e^{(2\pi x)}]$. When all data above the Coulomb barrier follow this curve, it implies in principle that the reaction cross sections can be described by Wong's approximation given by Eq. (7).

Although Canto *et al.* [40] have suggested that a deviation of experimental fusion functions, with respect to the $F_0(x)$, should be due to dynamic effects such as channel-couplings, it is not so clear if the same holds for the total reaction cross sections.

In any case, by considering this universal function reduction procedure for heavier targets, such as ^{58}Ni, ^{64}Zn, or even ^{209}Bi, where Coulomb breakup predominates over the nuclear breakup [38], larger reduced total reaction cross sections are obtained at energies around the Coulomb barrier for exotic nuclei (^{6}He and ^{8}B) followed by the weakly bound nuclei (^{6}Li,^{7}Li, ^{8}Li, and ^{9}Be) and then for the tightly bound nuclei (^{16}O and ^{4}He), as also obtained by the previous procedure to

reduce the cross section. This may indicate that, unlike for lighter targets, the breakup cross sections for these systems (or breakup + neutron transfer cross sections for the ^{6}He projectile) may likely be responsible for an appreciable part of the total reaction cross sections. As observed in Fig. 1 of Ref. [38], even for medium-mass targets such as ^{27}Al, where the Coulomb field is not so intense, the indication is that transfer and/or breakup cross sections might be a very important channel for ^{6}He. However, in contrast, this behavior is not observed for the light target ^{12}C, since the $F(x)$ function for weakly bound lithium and beryllium isotopes, for ^{6}He, and for the tightly bound nuclei ^{11}B and ^{16}O follow the same trend, indicating that breakup channels may not be important.

V. SUMMARY

We report here measurements and analyses of the elastic-scattering angular distributions of ^{8}B, ^{7}Be, and ^{6}Li on a ^{12}C target following a systematic investigation of the elastic scattering of weakly bound light nuclei. The measured elastic-scattering angular distributions can be reproduced with conventional WS potentials, double-folding model optical potentials, and a cluster-folding model in the case of the ^{8}B nucleus. The effect of breakup (continuum) on the elastic scattering was investigated for the weakly bound ^{8}B nucleus by performing CDCC calculations, and for this light ^{12}C target the effect can be considered negligible in the description of the elastic-scattering data. Breakup effects on the total reaction cross section were investigate by calculating the reduced reaction cross sections as a function of reduced energy for the lithium and beryllium isotopes as well as for the borromean nucleus ^{6}He, the proton halo nucleus ^{8}B, and the tightly bound ^{11}B nucleus on ^{12}C. All these systems have the same behavior in this description, indicating that for light systems the effects of the binding energy through breakup on the reaction cross sections likely are very small.

[1] E. F. Aguilera *et al.*, Phys. Rev. C **63**, 061603 (2001).
[2] L. R. Gasques *et al.*, Phys. Rev. C **67**, 024602 (2003).
[3] E. A. Benjamim *et al.*, Phys. Lett. B **647**, 30 (2007).
[4] M. Rodríguez-Gallardo, J. M. Arias, J. Gómez-Camacho, R. C. Johnson, A. M. Moro, I. J. Thompson, and J. A. Tostevin, Phys. Rev. C **77**, 064609 (2008).
[5] E. F. Aguilera *et al.*, Phys. Rev. C **79**, 021601 (2009).
[6] P. N. de Faria *et al.*, Phys. Rev. C **81**, 044605 (2010).
[7] T. Matsumoto, T. Egami, K. Ogata, Y. Iseri, M. Kamimura, and M. Yahiro, Phys. Rev. C **73**, 051602 (2006).

[8] A. Di Pietro *et al.*, Phys. Rev. C **69**, 044613 (2004).
[9] T. Matsumoto, E. Hiyama, K. Ogata, Y. Iseri, M. Kamimura, S. Chiba, and M. Yahiro, Phys. Rev. C **70**, 061601 (2004).
[10] I. Pecina *et al.*, Phys. Rev. C **52**, 191 (1995).
[11] G. Tabacaru *et al.*, Phys. Rev. C **73**, 025808 (2006).
[12] J. Lubian, T. Correa, E. F. Aguilera, L. F. Canto, A. Gomez-Camacho, E. M. Quiroz, and P. R. S. Gomes, Phys. Rev. C **79**, 064605 (2009).

[13] F. D. Becchetti, M. Y. Lee, T. W. O'Donnell, D. A. Roberts, J. J. Kolata, L. O. Lamm, G. Rogachev, V. Guimaraes, P. A. DeYoung, and S. Vincent, Nucl. Instrum. Methods Phys. Res. Sect. A **505**, 377 (2003).

[14] I. J. Thompson, Comput. Phys. Rep. **7**, 167 (1988).

[15] F. Michel and S. Ohkubo, Phys. Rev. C **72**, 054601 (2005).

[16] L. Jarczyk, J. Okolowicz, A. Strzalkowski, K. Bodek, M. Hugi, L. Lang, R. Müller, and E. Ungricht, Nucl. Phys. A **316**, 139 (1979).

[17] C. M. Perey and F. G. Perey, At. Data Nucl. Data Tables **17**, 1 (1976).

[18] L. C. Chamon, B. V. Carlson, L. R. Gasques, D. Pereira, C. De Conti, M. A. G. Alvarez, M. S. Hussein, M. A. Cândido Ribeiro, E. S. Rossi, and C. P. Silva, Phys. Rev. C **66**, 014610 (2002).

[19] L. R. Gasques *et al.*, Nucl. Phys. A **764**, 135 (2006).

[20] Z. Moroz *et al.*, Nucl. Phys. A **381**, 294 (1982).

[21] J. A. Tostevin, F. M. Nunes, and I. J. Thompson, Phys. Rev. C **63**, 024617 (2001).

[22] L. F. Canto, J. Lubian, P. R. S. Gomes, and M. S. Hussein, Phys. Rev. C **80**, 047601 (2009).

[23] P. R. S. Gomes, J. Lubian, I. Padron, and R. M. Anjos, Phys. Rev. C **71**, 017601 (2005).

[24] R. J. Smith, J. J. Kolata, K. Lamkin, A. Morsad, K. Ashktorab, F. D. Becchetti, J. A. Brown, J. W. Janecke, W. Z. Liu, and D. A. Roberts, Phys. Rev. C **43**, 761 (1991).

[25] R. E. Warner *et al.*, Phys. Rev. C **51**, 178 (1995).

[26] M. Milin *et al.*, Nucl. Phys. A **730**, 285 (2004).

[27] J. E. Poling, E. Norbeck, and R. R. Carlson, Phys. Rev. C **5**, 1819 (1972).

[28] J. E. Poling, E. Norbeck, and R. R. Carlson, Phys. Rev. C **13**, 648 (1976).

[29] D. E. Trcka, A. D. Frawley, K. W. Kemper, D. Robson, J. D. Fox, and E. G. Myers, Phys. Rev. C **41**, 2134 (1990).

[30] A. Barioni *et al.*, Phys. Rev. C **80**, 034617 (2009).

[31] L. Jarczyk, B. Kamys, A. Strzałkowski, A. Szczurek, M. Godlewski, J. Lang, R. Müller, and J. Sromicki, Phys. Rev. C **31**, 12 (1985).

[32] J. J. Kolata and E. F. Aguilera, Phys. Rev. C **79**, 027603 (2009).

[33] E. F. Aguilera, I. Martel, A. M. Sánchez-Benítez, and L. Acosta, Phys. Rev. C **83**, 021601 (2011).

[34] C. Y. Wong, Phys. Rev. Lett. **31**, 766 (1973).

[35] E. B. Carter, G. E. Mitchell, and R. H. Davis, Phys. Rev. **133**, B1421 (1964).

[36] P. Gomes, L. Canto, J. Lubian, and M. Hussein, Phys. Lett. B **695**, 320 (2011).

[37] L. Canto, P. Gomes, J. Lubian, L. Chamon, and E. Crema, Nucl. Phys. A **821**, 51 (2009).

[38] J. Shorto, P. Gomes, J. Lubian, L. Canto, S. Mukherjee, and L. Chamon, Phys. Lett. B **678**, 77 (2009).

[39] P. Charles, F. Auger, I. Badawy, B. Berthier, M. Dost, J. Gastebois, B. Fernandez, S. M. Lee, and E. Plagnol, Phys. Lett. B **62**, 289 (1976).

[40] L. F. Canto, P. R. S. Gomes, J. Lubian, L. C. Chamon, and E. Crema, J. Phys. G: Nucl. Part. Phys. **36**, 015109 (2009).